A Model of Cross-Bridge Attachment to Actin in the A·M·ATP State Based on X-Ray Diffraction from Permeabilized Rabbit Psoas Muscle

Jin Gu, Sengen Xu, and Leepo C. Yu
National Institute of Arthritis, Musculoskeletal and Skin Diseases, National Institutes of Health, Bethesda, Maryland 20892 USA

ABSTRACT A model of cross-bridges binding to actin in the weak binding A·M·ATP state is presented. The modeling was based on the x-ray diffraction patterns from the relaxed skinned rabbit psoas muscle fibers where ATP hydrolysis was inhibited by N-phenylmaleimide treatment (S. Xu, J. Gu, G. Melvin, L. C. Yu. 2002. *Biophys. J.* 82:2111–2122). Calculations included both the myosin filaments and the actin filaments of the muscle cells, and the binding to actin was assumed to be single headed. To achieve a good fit, considerable flexibility in the orientation of the myosin head and the position of the S1-S2 junction is necessary, such that the myosin head can bind to a nearby actin whereas the tail end was kept in the proximity of the helical track of the myosin filament. Hence, the best-fit model shows that the head binds to actin in a wide range of orientations, and the tail end deviates substantially from its lattice position in the radial direction (~60 Å). Surprisingly, the best fit model reveals that the detached head, whose location thus far has remained undetected, seems to be located close to the surface of the myosin filament. Another significant requirement of the best-fit model is that the binding site on actin is near the N terminus of the actin subunit, a position distinct from the putative rigor-binding site. The results support the idea that the essential role played by the weak binding states M·ATP ↔ A·M·ATP for force generation lies in its flexibility, because the probability of attachment is greatly increased, compared with the weak binding M·ADP·P_i ↔ A·M·ADP·P_i states.

INTRODUCTION

It is well established that the energy source of muscle contraction is ATP hydrolysis by actomyosin. The generally accepted biochemical scheme of intermediate states in the catalytic cycle is (Scheme 1):

$$\begin{array}{ccccccc} \text{M·ATP} & \rightleftharpoons & \text{M·ADP·P}_i & \rightleftharpoons & \text{M·ADP} & \rightleftharpoons & \text{M} \\ \updownarrow & & \updownarrow & & \updownarrow & & \updownarrow \\ \text{A·M·ATP} & \rightleftharpoons & \text{A·M·ADP·P}_i & \rightleftharpoons & \text{A·M·ADP} & \rightleftharpoons & \text{A·M} \end{array}$$

Scheme 1

Where M = myosin and A = actin. For those states of myosin with bound ATP or hydrolysis products (A·M·ATP or A·M·ADP·P_i), the affinity between actin and myosin is low (the weak binding states); for those states without nucleotide or with ADP (A·M or A·M·ADP), the affinity is greatly increased (the strong binding states). It is thought that force is generated in the transition of weakly to strongly bound states (Eisenberg and Hill, 1985).

As the function of muscle is to convert the chemical energy from ATP hydrolysis to generate physical displacement, some structural changes at the molecular level have been expected. Therefore, it is critical to follow structural changes in myosin and actin as hydrolysis proceeds through its cycle.

Submitted January 3, 2001, and accepted for publication January 4, 2002.

Address reprint requests to Jin Gu, National Institutes of Health, Building 50, Room 1349, Bethesda, MD 20892-8024. Tel.: 301-496-6723; Fax: 301-402-0009; E-mail: jingu@helix.nih.gov.

0006-3495/02/04/2123/11 $2.00

The atomic structures of the myosin head (S1) have revealed ligand-dependent differences which may very well correspond to changes induced by ATP hydrolysis in the actomyosin complex (Rayment et al., 1993a, 1996; Fisher et al., 1995; Smith and Rayment, 1996; Dominguez et al., 1998; Houdusse et al., 1999, 2000). However, crystal structures of S1 and the actin monomer alone do not necessarily reveal the in vivo structural changes that lead to force generation. It has been recognized that to generate force, some strain (hence some structural distortion) must be sustained by the links formed by the cross-bridges between the filaments. Because of the mismatch between the periodicities of the filaments, there is a distribution of strains sustained by the links. Therefore, a technique that can provide information about the distributions and orientations of the cross-bridges in the filament lattice during ATP hydrolysis is critical. X-ray diffraction from permeabilized muscle cells, the technique used in the present study, is one of the few techniques that reveal the structures as they occur in muscle cells, albeit at relatively low resolution.

Previously, we have shown that with myosin not attached to actin, among the four intermediate states (Scheme 1), only the state M·ADP·P_i exhibits a well ordered myosin filament structure; the myosin heads are arranged in an helical array surrounding the filament backbone (Xu et al., 1997, 1999). The other detached states exhibit a highly disordered structure. For the states involving actin-myosin interactions, the high-affinity states of A·M (rigor state) and A·M·ADP have been studied extensively and well characterized (e.g., Huxley et al., 1967; Kim et al., 1998). The myosin heads in these states are attached to actin in a uniform orientation with respect to the actin filaments.

Considerable information is available on the structural, biochemical, and mechanical properties of the two weakly

bound states A·M·ATP and A·M·ADP·P_i. These two states play a critical role in force generation. If they are blocked, force can not be generated (Brenner et al., 1991; Kraft et al., 1995), even though in a relaxed muscle under physiological conditions, the population of weakly attached cross-bridges is estimated to be ~10%. Thus far, however, structural and mechanical studies on the weakly bound states have been obtained from a mixture of the two states in a relaxed muscle. Because ATP hydrolysis brings about a change in the myosin filament structure (Xu et al., 1999) and in the actin-myosin affinity (White et al., 1997), it is highly probable that the structures of these two attached states are distinct.

Because of their fast kinetics, it has been difficult to distinguish between the two weakly bound states. However, when the myosin is reacted with N-phenylmaleimide, ATP hydrolysis is inhibited (Barnett et al., 1993; Xu et al., 1998; Xie et al., 1999), i.e., in the presence of MgATP, the myosin is kept only in the state with bound ATP. This intervention enabled us to isolate the A·M·ATP and M·ATP from the rest of the cycle. We have obtained x-ray diffraction data from rabbit psoas muscle chemically modified by N-phenylmaleimide (Xu et al., accompanying paper). The purpose of this paper is to model the filament lattice in the A·M·ATP state based on the experimental data obtained by Xu et al. (2002).

With the assumption that only one head of the cross-bridge is attached to actin at any given time and the shape of S1 following that of Rayment et al. (1993), the present modeling requires that there is a wide range of orientation of the attached myosin head with respect to the actin filament. The unbound head, on the other hand, appears to be located close to the myosin filament backbone. The end of the head at the S1-S2 junction remains in the vicinity of the helical track of the myosin filament, but there is a high degree of fluctuation, mostly in the radial direction. Last, the binding site on the actin subunit is at a higher radius than the putative rigor-binding site (Rayment et al., 1993b; Schroder et al., 1993; Mendelson and Morris, 1997).

Preliminary results have been presented previously (Gu et al., 2000).

METHODS

During the course of this study, various assumptions were systematically tried to fit the x-ray data. Initially, we investigated models with no attachment (only ordering around the thick filament), and models with uniform orientations for attachment. The results (see below) did not explain the experimental data. Eventually, it was concluded that attachment orientation could not be constrained to be uniform.

The main assumptions and calculation procedures used in the present modeling are summarized as following: 1) the S1 was simplified from the atomic structure (Rayment et al., 1993) and the attachment was single headed (Appendix (a)); 2) 100% of the single myosin heads were attached under the low ionic strength condition (Appendix (a) and (b)); 3) the position of the binding site on actin was varied, but was the same for each subunit (Appendix (c)). The binding site on myosin that binds actin was defined by a small sphere corresponding to the heavy chain segment from Pro^{529} to Lys^{553} in the crystal structure (Rayment et al., 1993a) (Appendix (b)). The myosin site was not varied in the calculations; 4) the myosin heads were constrained to bind to a nearby actin subunit (Appendix (d)), forming a binding pair (Appendix (f)); for models A and B the nearest actin subunit from the myosin lattice point was chosen to form "binding pairs." For model C, the actin subunit was selected at a distance closest to the chord length of the myosin head (from the tail end to the binding site on the motor domain, ~137 Å). The orientation of the attachment was not constrained. 5) The position of the myosin head on the helical track of the thick filament, or the shape of the myosin head was adjusted to accommodate the various distances required by the binding pair. For model A: the radial position R of the S1-S2 junction at the helical lattice point was allowed to deviate ΔR whereas the shape of myosin head remained unchanged; for model B, the myosin head changed its conformation approximately at the converter region (Houdusse et al., 1999), such that the angle (ψ) between the light chain binding domain and the binding site in the motor domain was a variable (Fig. 1), but the position of the tail end was kept at the helical lattice point; for model C, as in model A, binding was accomplished by adjusting the radial position of the S1-S2 junction at the myosin lattice point, while keeping the shape of S1 unchanged. 6) To improve the fitting, some extra mass associated with the attached head was found necessary, which was assumed to be the detached myosin head (H2) (Appendix (f)).

Model parameters and calculation procedures are explained in detail in Appendices (e), (h) and (i).

RESULTS

The calculated layer lines and the experimental data are matched well (Fig. 2). The simulated diffraction pattern from the model includes the six myosin layer lines (MLL1 ~ MLL6) as well as the prominent actin layer lines. For the case of 100% attachment (i.e., all the cross-bridges are attached with one head), the *R*-factor, which is defined as: $R = (\Sigma|I_{cal} - I_{exp}|/\Sigma I_{exp})$, for the six myosin-based layer lines (MLL1 ~ MLL6) is 0.045; and for actomyosin layer lines (ALL1 and ALL6) are 0.067 and 0.025.

Models with uniform attachment orientations can not explain the experimental data

During the initial phase of the study, the possibility of a model with uniform orientation for attachment was tested. Regardless of the range of attachment angles used and the position of the binding site, there was no contribution to the myosin-layer line intensities and the actin-layer lines were too strong (Fig. 3). Therefore, the orientation of the attachment can not be uniform in the weak binding state of A·M·ATP.

The binding site on actin for the A·M·ATP state

The first myosin-layer line (MLL1) has two peaks. Regardless of the models we used, the position of the first peak was found to depend on the distance of the myosin heads from the axis of the myosin filament. Because the myosin head is connected to the actin subunit, the first peak is affected by the position of the binding site on the actin filament. The

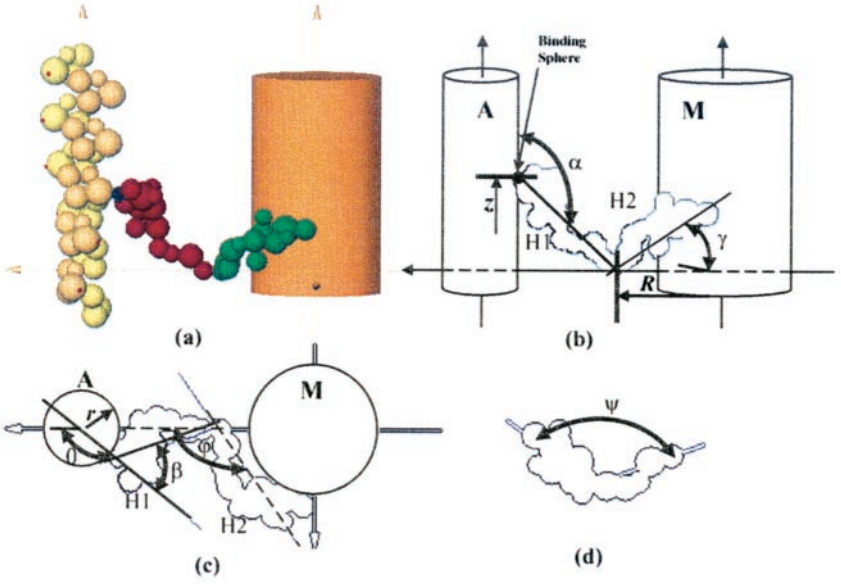

FIGURE 1 Schematic representations of the assumptions and parameters used in computations. The myosin head shape is based on the crystal structure of S1 (Rayment et al., 1993a). Each head is modeled as 16 spheres with radii in the range of 9.37 to 17.60 Å (for details see Methods). The small sphere in black denotes the binding sphere to actin (corresponding to the heavy chain segment from Pro^{529} to Lys^{553} in the S1 crystal structure). The actin filament is calculated as left-handed close to 13/6 helix with a pitch of 361 Å. The monomer is composed of four spheres representing each domain of the actin crystal structure (Kabsch et al., 1990; Squire et al., 1993). The length of filaments included in the calculations was 2165 Å (= 144.3 Å × 15 crowns for the myosin filament and = 361 Å × 6 repeats for the actin filament); the lattice spacing d_{10} = 404.5 Å. It is assumed that only one of the two heads (H1) of the cross-bridge is bound to actin forming a link between the filaments (*a*). The other head H2 is detached and tethered to H1 at the tail end. H1 binds to an actin subunit at a specific site (the red small point on the surface of the actin monomer) with tilt angle α and slew angle β relative to the axis of the actin filament (*b* and *c*). The specific site is located by $(r + \Delta r, \theta + \Delta\theta, z + \Delta z)$, in which the coordinates (r, θ, z) are labeled to be at the rigor contact point of the actin with attached myosin. The second head (H2) originates from the same position as H1 with slew angle φ and tilt angle γ to the plane perpendicular to the filaments (*b* and *c*: side and projection views). Starting from every helical lattice point at *R* from the axis of the myosin filament, an actin monomer is selected to form a binding pair. The search consisted of an area ±216 Å in the axial direction and ±60° in the azimuthal direction. Three criteria were used: for models A and B, the nearest actin subunit from the myosin lattice point was chosen to form the binding pairs. For model C, instead of the nearest neighbors, the actin subunit was selected at a distance closest to the chord length of the myosin head (from the tail end to the binding site on the motor domain, ~137 Å). Because of the mismatch of the periodicities of the filaments, the distances between the binding pairs differ from one another. Three different adjustments were used to fit the myosin head into the lattice space. For model A, the radial position *R* of the S1-S2 junction at the lattice point, initially at 95 Å from the axis of the myosin filament, is allowed to deviate from the helical track whereas the shape of myosin head remains unchanged. For model B, H1 changes its conformation approximately at the converter region (Houdusse et al., 1999), such that the angle (ψ) is a variable as shown in (*d*), but the position of the tail end is kept at 95 Å from the axis of the myosin filament. Model C lets the chord length of the myosin head (~137 Å) select the corresponding actin for the binding pair. Subsequently, binding was accomplished by adjusting the radial position *R* of the S1-S2 junction at the myosin lattice point.

best fitted profile of the MLL1 for the A·M·ATP state requires a binding site at a radius of 45 ± 2 Å from the axis of the actin filament. The putative binding site on actin as derived from fitting the S1 atomic structure into the mass envelope of decorated actin filament in the electron mircrograph was at ~26Å (Rayment et al., 1993b) or ~30Å (Mendelson and Morris, 1997) for the rigor state. The putative binding site on actin was defined by us in the same way as in our modeling, i.e., it is the position where the binding sphere at the tip of the simplified myosin head touches the actin surface.

In addition to the radial position being different from the rigor site, other coordinates of the binding site also differed. The clue came from the experimental observation that the 59 Å actin layer line (ALL6) is insensitive to weak binding of cross-bridges (Fig. 7 in Xu et al., (2002); (Xu et al., 1997)). The site in the cylindrical coordinates was required to shift from the putative rigor site by: Δr = 19 Å, $\Delta\theta$ = 38°, and Δz = 23 Å, whereas there is a wide range of the orientation of the bound myosin head (Fig. 4). Fig. 5 shows the experimental data of the 59-Å layer line and the calculated data of the model. The modeled curve (Fig. 5, *solid line*) almost overlaps the calculated curve (Fig. 5, *dashed line*) of an actin filament with no heads attachment, i.e., the modeled curve is insensitive to binding. Similar results were obtained for all three models we considered.

As a contrast, the calculated profile of ALL6 (Fig. 5, *dashed-dot line*) would be much stronger than the experimental data (Fig. 5, *dots*) and would peak at a different position, if the myosin heads were bound to the putative rigor site even with the same wide range of attachment orientations. If the myosin heads were to maintain the same

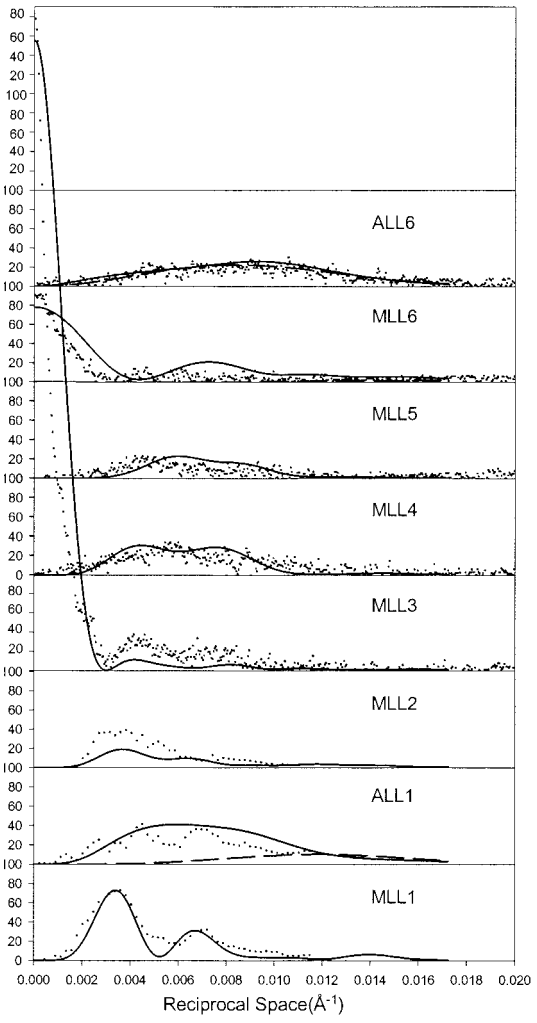

FIGURE 2 Profiles (*solid lines*) of the calculated layer lines from the best fitted model compared with the experimental data (*dots*). With the assumption of 100% single head attachment, the calculated layer lines fit the experimental data closely except in MLL2. The parameters for the cross-bridge population in the final model were: $R+\Delta R = 78\sim139$ Å, $r = 45 \pm 2$ Å, $\alpha = 61\sim131°$, $\beta = -80\sim74°$, $\varphi = 125 \pm 3°$, and $\gamma = \pm 19.5°$. The R factor for six myosin-based layer lines (MLL1 ~ MLL6) is 0.045; and for actomyosin layer lines (ALL1 and ALL6) $R = 0.067$ and 0.025. In 0% attachment, the calculated layer lines (*dashed lines*) show only ALL1 and ALL6.

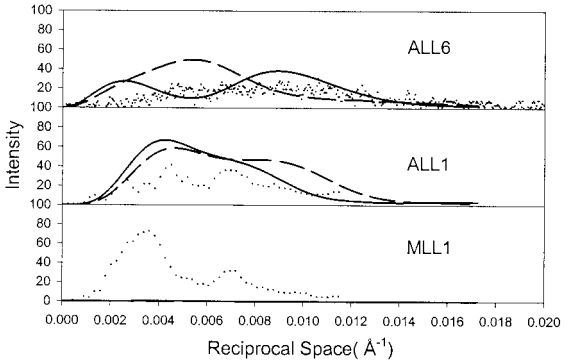

FIGURE 3 Profiles of the calculated layer lines from bound myosin heads in uniform orientation around the actin filament. Experimental data are in dots. Orientation of the heads was assumed to be with $\Delta\alpha = -23$, $\Delta\beta = 22$ different from that of heads in the rigor. This calculation shows that uniform binding either at the putative rigor site (*solid lines*) or at the binding site discussed below (*dashed lines*) (Fig. 4) only contributes to actin layer lines, but not to the myosin layer line. Therefore, myosin heads could not bind to actin with the uniform orientations.

uniform rigor orientation but bound at the weak binding site, the profiles of ALL6 and ALL1 also become overly strong and rigor-like (data not shown). Thus, the result on the location of the binding site on actin for A·M·ATP is supported by the intensity distributions of the myosin and the actin layer lines.

A more precise location of the binding site in the atomic structure of actin can be derived by shifting the S1 in the cylindrical coordinates with $\Delta r = 19$ Å, $\Delta\theta = 38°$, and $\Delta z = 23$ Å, respectively, with the rigor model of Rayment et al. (1993b) as the origin. The weak binding site is shown approximately to be near both the four residues at N-terminal (Asp^1 to Glu^4) and the loop segment Ala^{97} to Glu^{100} of actin. By examining the interface between S1 and actin, a small loop from Pro^{543} to Thr^{546} of S1 is close to both these regions of actin, whereas a large loop Gly^{627} to Phe^{646} missing from the x-ray structure of S1 is also nearby (Fig. 4 *A*). We could not model the missing loop because its location is not known. However, our conclusion that the binding interface of S1 is located at 45 Å from the axis of the actin filament would place the missing loop within the reach of the N terminus of actin.

The range of orientations of the bound myosin heads

The ranges of attachment angles, in azimuthal angles (β), and the axial spread for the three models are listed in Table 1. To fit the variable distances for the binding pairs, the three models made different adjustments. For model A, the radial distance ($R + \Delta R$) of the center of the last sphere of S1 ranged between 78 and 139 Å from the axis of the myosin filament. For model B, with the head-tail junction $R = 95$ Å which is the best fit, the range of angle ψ pivoted at the converter domain within the myosin head was between 78 and 156°. For model C, the radial position from the helical track ranged between 91 and 146 Å.

Extra mass associated with the attached myosin head

The MLL1 has two peaks at 0.0033 and 0.0069 $Å^{-1}$. The amplitude of the second peak further away from the meridian is approximately one-third of the first peak (Xu et al., accompanying paper). Model calculations found that the weakly attached myosin heads contribute mainly to the first

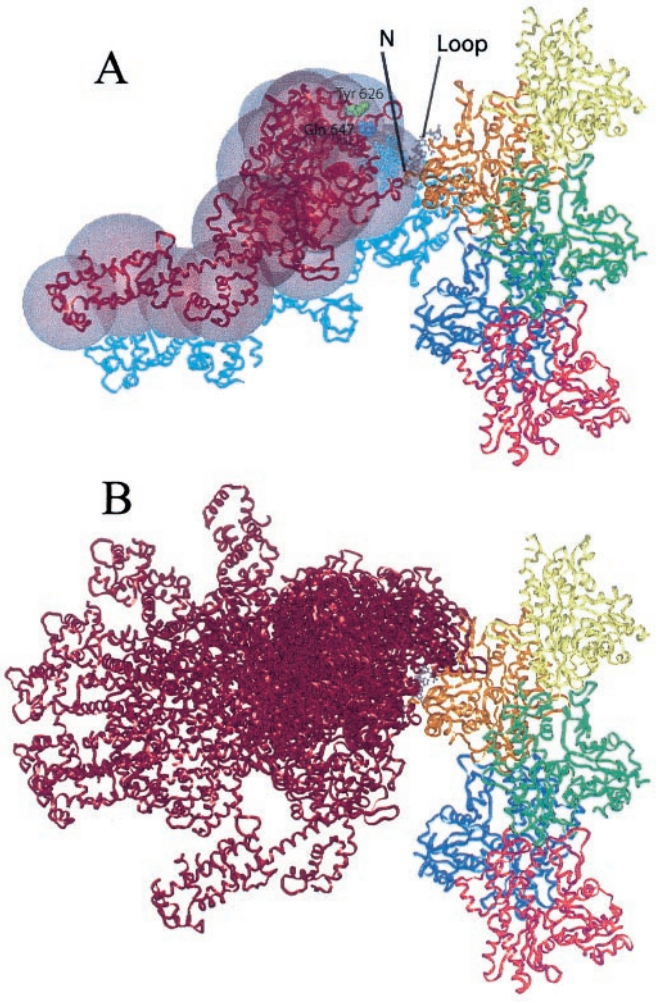

FIGURE 4 (*A*) Different sites for weak binding and for rigor: the binding site on actin for the A·M·ATP state (S1 in *dark red*) is indicated at a position near the N terminus and a loop (*gray*) of the actin subunit. The S1 in rigor is indicated by *blue*. The positions differ by a radial translation $\Delta r = 19$ Å, azimuthal rotation $\Delta\theta = 38°$, and vertical translation $\Delta z = 23$ Å. The simplified S1 used in our calculations (*spheres in light red*) is overlapped with the crystal structure of S1. (*B*) Superposition of seven typically bound heads (*red*) in the A·M·ATP state in a longitudinal view. The range of the tilt angle α is between 61 and 131°; the slew angle β, between −80 and 74°.

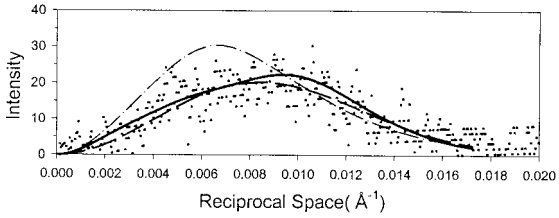

FIGURE 5 The binding site on actin is required to be near the N terminus. Experimental data of ALL6 at 59 Å are shown in dots. The layer line (*solid line*) based on model A with the binding near the N terminus shows little difference from the layer line (*dashed line*) calculated from a bare actin filament model (Squire et al., 1993). In contrast, the dash-dot line illustrates the discrepancy if the heads were bound to actin at the same site as the rigor binding (Rayment et al., 1993b), even if the range of binding angles was kept unchanged from model A. Therefore, it was necessary to shift the binding site to the N terminus of actin for the state of A·M·ATP.

peak. The amplitude of the second peak was invariably too low without considering some extra mass associated with the attached head. Furthermore, layer lines MLL3, MLL4, and MLL6 also could not be fitted well. It was therefore necessary to consider that some additional mass is in a helical distribution when the first head was bound. We assumed the extra mass to be the second head of the cross-bridge. For the best fit, φ and γ were found to be $125 \pm 3°$ and $\pm 19 \pm 0.5°$ (Appendix (g) and Fig. 1) so that the angle between the first and second heads is distributed between 60 and 160°. The mean is 113°. This results in the radial position of the second head to be close to the surface of the myosin filament. The fit is not as good if the angle between the two heads were fixed. Using the results derived for model A as an example, Fig. 6 illustrates the effects of the second head on the myosin layer lines.

The three models become distinct with the consideration of the second head

All three models yielded similar characteristics in the calculated diffraction patterns, if one only considers single-headed cross-bridges. However, with the inclusion of the extra mass (second head), the three models show distinct effects on the MLL1, MLL3, MLL4, and MLL6. The conformation adjustment in the converter domain (model B) does not fit very well for the MLL3, MLL4, and MLL6 although the MLL1 can be fitted. Fig. 7 shows the profiles of the calculated MLL1 as a result of adjustments for models A, B, and C. For model B, even using an additional parameter, the fraction of the second heads that follow the first heads, the match remains poorer when compared with model A. The fit of the model C on most of the myosin-based layer lines and the first actin layer lines is not as good

TABLE 1 Results in attachment orientations derived for models A, B and C

Model	A	B	C
α (°)	61 ~ 131	60 ~ 129	50 ~ 131
β (°)	−80 ~ 74	−80 ~ 70	−80 ~ 67
ψ (°)	134.9	78 ~ 156	134.9
$R + \Delta R$ (nm)	7.8 ~ 13.9	9.5	9.1 ~ 14.6

The resultant attachment orientations of the myosin heads are expressed in the tilt angle α and the slew angle β relative to the axis of the actin filament. For model B, there is a distribution in ψ, the angle between the light chain domain and the binding site in the motor domain of S1. $R + \Delta R$ is the radial position of the S1-S2 junction (the last sphere of the modeled S1 in Fig. 1) from the axis of the myosin filament.

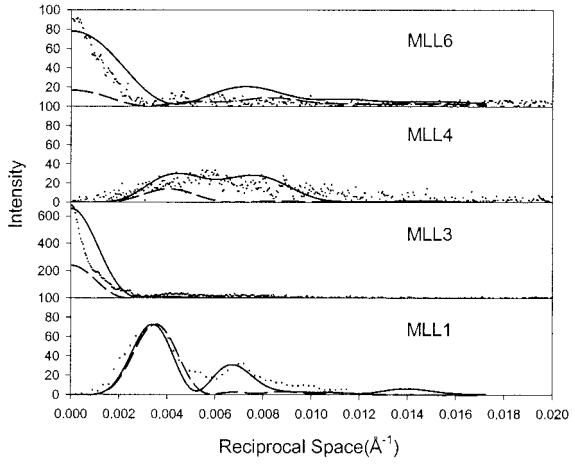

FIGURE 6 The amplitude of the second peak of the layer line MLL1 (*dashed line*) was invariably too low without considering extra mass associated with the attached head H1, if the second head H2 of the cross-bridge was in complete disorder (i.e., no contribution to intensities). With the inclusion of H2, not only the MLL1 but also the MLL3, MLL4, and MLL6 layer lines (*solid lines*) fit very well with the experimental data (*dots*). The population of H2 is distributed in an approximate helical arrangement close to surface of the myosin filament. Although the shown curves are from the best-fitting model, model A, the other two models also require H2 to enhance the second peak (data not shown).

as the one obtained for model A. Therefore, it is concluded that model A is the model of choice (Fig. 2).

The results are not significantly affected by displacement perturbations along the thick filament

On the meridian, there are several reflections, the 21.5-nm reflection being the most prominent, "forbidden" by the selection rules for an integral three-stranded helical filament. The most credible explanation for the forbidden reflections was the displacement perturbation of the cross-bridges along the thick filament (Squire et al., 1982; Stewart and Kensler, 1986; Malinchik and Lednev, 1992). We have examined the effects of the perturbations on our model. In the A·M·ATP state, the amplitude of the MLL1 intensity increases ~15% when the perturbation is applied. The changes in MLL1 and MLL3 can be compensated by slightly decreasing the tilt angle for ~3°. Regardless, there is no change in the peak positions of the intensity profiles when the 21.5-nm and other forbidden reflections appear on the meridian. Furthermore, the perturbation does not affect the 5.9-nm layer line.

DISCUSSION

The experimental features placed specific requirements on the modeling. The weak layer line intensities required that the orientation of binding be nonuniform. The increase in

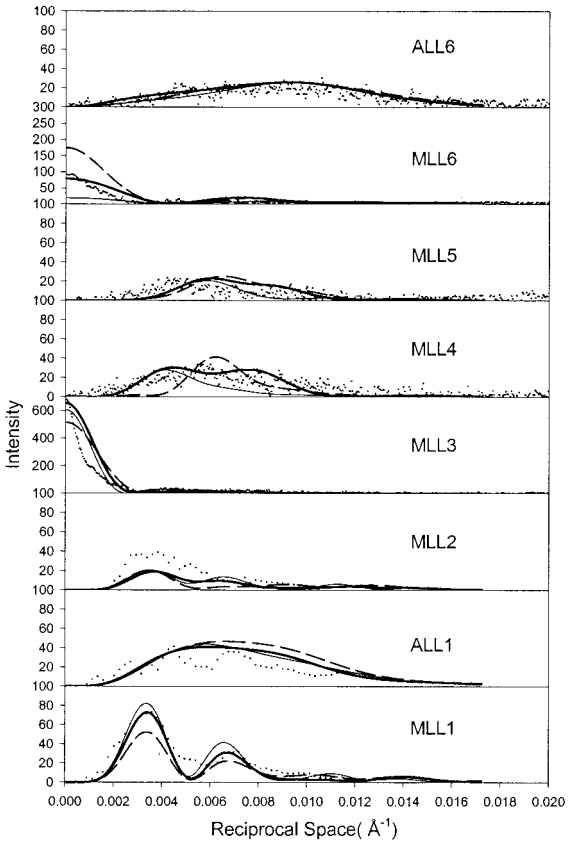

FIGURE 7 The layer lines best fitted by the three models A (*thick solid lines*), B (*thin solid lines*), and C (*dashed lines*) compared with experimental data (*dots*). The fit by model A is superior. Parameters used in model A: the same as in Fig. 2. Model B: $R = 95$ Å, $r = 45$ Å, $\alpha = 60\sim129°$, $\beta = -80\sim70°$, $\psi = 78\sim156°$, $\varphi = 125°$, and $\gamma = \pm19.5°$. Model C: $R = 91\sim146$ Å, $r = 45$ Å, $\alpha = 50\sim131°$, $\beta = -80\sim67°$, $\varphi = 125°$, and $\gamma = \pm19.5°$.

myosin layer lines required some degree of helical symmetry for the disposition of attached myosin heads. The inclusion of the second head was needed to fit the second peak on the first myosin layer line. The binding site on actin is supported by two sets of layer lines. Considering that only seven parameters for each model were used to describe the three-dimensional (3-D) disposition of the myosin heads and the binding site on actin, the model was well constrained by the experimental data.

The binding site on actin for the A·M·ATP state differs from that for the rigor state

One of the most interesting conclusions is that the binding site on actin is at a higher radius from the actin filament axis than that of the putative site for the rigor state (Rayment et al., 1993b; Schroder et al., 1993; Mendelson and Morris, 1997). It should be emphasized that this conclusion is based not only on the intensity distributions of the actin layer lines, but also on the peak positions of the myosin layer

lines. Biochemical and structural evidence has for some time suggested that the N terminus is involved in the weak binding of S1 to actin (Sutoh, 1982; Rayment et al., 1993; Lehman et al., 1994). The present study, for the first time, provided information for in vivo binding that supports the original suggestion. The present result also resolves one of the long-held puzzles that the weak binding of cross-bridges enhances the intensity of ALL1, but not ALL6 at 59 Å (Xu et al., 1997).

The extra mass associated with the attached myosin head reveals the location of the second head of the cross-bridge

The whereabouts of the second head have thus far remained unclear. However, the present results strongly suggest that the required extra mass is the detached head, as it is helically distributed and it follows the same periodicity on the myosin filament as the attached head. It is noteworthy that the angle separating the two heads is greater than 60°, indicating that they are mostly splayed. Our result is consistent with the tomographic 3-D reconstruction of the isometrically contracting insect flight muscle (Taylor et al., 1999). A two-headed model has also been proposed by Linari et al. (2000) and Juanhuix et al. (2001) for actively contracting muscle. The two heads in our model are assumed to be equivalent, switching alternately between the attached/detached state.

The results could not be explained by a mixture of two populations with fixed orientations

It might be argued that the observed diffraction patterns could originate from a simple mixture of two populations with different stereospecific symmetries. One population could originate from myosin heads well ordered on a helical track surrounding the myosin filament so that the myosin layer lines are enhanced, whereas a second population could originate from binding on the actin filament in a uniform orientation enhancing the actin layer lines. This is highly unlikely for two reasons: one is that the intensity of MLL1 would be stronger than that of MLL3 on the meridian if the myosin heads were ordered on the normal myosin helix (Malinchik et al., 1997). On the contrary, the intensity of the MLL3 is stronger in the A·M·ATP state in the present case. The other reason is that the intensity of the ALL6 would be too strong if binding to the actin filament is uniformly oriented, e.g., in the rigor state (Gu and Yu, 1999) or at a fixed orientation (Fig. 3).

Significance to contraction mechanism

One of the major characteristics of the A·M·ATP state is the considerable flexibility in the actomyosin complex as indicated by the wide range of attachment angles and radial positions from the myosin filament surface. We propose that it is this high degree of flexibility that renders the A·M·ATP state being physiologically significant for force generation in muscle. It has been shown that the myosin molecules in the M·ADP·P_i state are arranged in a well ordered array (Xu et al., 1999). Because the diffraction patterns from this state are sharp, the myosin molecules do not deviate significantly from their lattice points (Lowy et al., 1991; Malinchik et al., 1997). In addition, preliminary results indicate that the near crystalline nature is not perturbed when the low-affinity state A·M·ADP·P_i is formed (Xu et al., 2001). Because of the incommensurate filament repeats, few cross-bridges could attach to actin under this condition. However, the probability for attachment is greatly increased for myosins in the M·ATP state, forming the A·M·ATP state with multiple orientations. Therefore, the A·M·ATP state may serve as a "recognition state," whereby hydrolysis and force generation can proceed along the attached pathway.

The difference in the binding sites on actin is consistent with recent biochemical studies of Hansen et al. (2000), which suggested a transition at the N terminus on actin between the weakly and strongly bound states. It is possible that the interaction interface increases with successive steps in the hydrolysis pathway (Scheme I, top tier). Further experiments will be necessary to explore such possibilities.

In summary, the x-ray diffraction patterns obtained from the relaxed muscle with myosins in the A·M·ATP state suggest that in addition to the flexible, multiple orientations of attachment, there is a significant difference in the binding sites on actin between the rigor state and the weak binding state. The modeling also reveals that the detached head of the myosin is distributed close to the myosin filament backbone.

APPENDIX

(a) Simplifying assumptions

At 5°C, the fraction of cross-bridges bound at ionic strength = 27 mM is estimated to reach as high as 80%, and at 170 mM, the fraction is ~30%. The difference pattern (Fig. 1 *C* in Xu et al., 2002) between the low and high ionic strengths shows directly the intensity changes associated with increased attachment. Some components are reduced to noise level after the subtraction (e.g., the second peak on MLL1). However, such components turned out to contain critical information on the distribution of the second myosin head. Hence, the difference pattern was not used for the modeling. Instead, the present modeling is to find a best fit for the diffraction pattern shown in Fig. 1 *A* of Xu et al. (2002). A set of contiguous vertical cuts with narrow width (five pixels) was made to the pattern to separate the first, the second myosin based and the first actin based layer lines. The reconstructed layer lines are shown in Fig. 2 in dots and in Fig. 7 of Xu et al. (2002).

Because a large fraction is bound at the low ionic strength and the detached myosin in the M·ATP state is disordered (not contributing to layer line intensities), we made the simplifying assumption that at ionic strength = 27 mM, 100% of the cross-bridges are attached to actin with single-head attachment.

Based on the low affinity of the weak binding states as indicated by the biochemical data (Chalovich et al., 1981; Chalovich and Eisenberg, 1982,

1986; White et al., 1997) and electron microscopic observations (Frado and Craig, 1992), it is assumed that only one of the two heads attaches to an actin subunit at any given time. The attached head is designated as H1 whereas the detached one is H2 (Fig. 1). The two heads are assumed to tether at the tail end (i.e., the last sphere at the end of the head in the model).

(b) The model of S1 and the myosin filament

A 3-D grid (30 Å) was used to bin the atomic structure of S1 (Rayment et al., 1993a) and convert the resulting 3-D bins (cubes) into spheres. A sphere was drawn with the same mass and with its center coinciding with the center of mass found within the cube. All spheres were brought to the same density by adjusting sphere radius. As a result, the myosin head (S1) was represented by 16 spheres with radii in the range of 9.37 to 17.60 Å.

The site on the myosin head that binds actin was defined by a small sphere corresponding to the heavy chain segment from Pro^{529} to Lys^{553} in the crystal structure (Rayment et al., 1993a). This is shown in black in Fig. 1.

The myosin filament structure was assumed to consist of a smooth cylindrical backbone and a three-stranded 9/1 helix consisting of myosin cross-bridges projecting outward with a repeat of 433 Å. The distance between successive crowns of myosin heads was equal to 144.3 Å. The diameter of the backbone shaft was assumed to be 150 Å.

The attached head is designated as H1 and the detached one is H2 (Fig. 1.) The two heads are assumed to tether at the tail end (i.e., the last sphere at the end of the head in the model).

(c) The model of the actin subunit and the actin filament

The modeled actin monomer consists of four spheres of radii 16.81, 10.53, 14.92, and 14.26 Å, respectively, representing the four subdomains 1, 2, 3, and 4 of the actin crystal structure (Kabsch et al., 1990). The coordinates of the spheres were taken from Squire et al. (1993) (Fig. 1 *a*). The binding site on actin is assumed to be the same on every actin subunit (i.e., the binding is site-specific). At the start of the search routine, the binding site is assumed to be on the actin surface at a radius of 26 Å from the axis of the actin filament. The latter position corresponds to that for the rigor binding as proposed by Rayment et al. (1993b). The binding position as a function of the three polar coordinates was allowed to change as a part of the search routine. The final selection was determined by a best fit of the calculated actomyosin layer lines and the sixth actin filament layer line at 59 Å to the experimental data (see Results).

The actin filament was calculated with the assumption of being a left-handed close to 13/6 helix with a pitch of 361 Å.

(d) The filament lattice

In the transverse section of the A-band, each myosin filament is surrounded by six actin filaments; and each actin filament is surrounded by three myosin filaments. As there are three pairs of myosin heads at each crown level converging on one actin filament, an angular sector of 120° in the azimuthal direction on the actin surface is allowed for each myosin head to bind. The orientation of the actin filaments in the sarcomere is assumed to be identical, as previously suggested by Hirose and Wakabayashi (1988). The length of filaments included in the calculations was 2165 Å (= 144.3 Å × 15 crowns for the myosin filament and = 361 Å × 6 repeats for the actin filament).

Other dimensions used in the model are as follow: the lattice size d_{10} = 404.5 Å. The azimuthal angle at the start of the myosin filament relative to that of the actin filament was kept constant. During the early phase of our study, this azimuthal angle was varied, but it was found that changes in this parameter had little effect on the layer lines because of the long length of filaments used in our calculations.

Some simplifying assumptions have been made in modeling the filament structures, i.e., the associated proteins are ignored in the calculations. Myosin is the main component of the thick filament. Because of its sheer size, it is the main contributor to the x-ray diffraction patterns observed by Xu et al. (2002). The C-protein, a thick filament associated protein, accounts for ~2% of the protein mass in a vertebrate muscle, and makes observable contributions only on the meridian at a different index (43.5–44.2 nm) compared with the myosin helix (Rome et al., 1973). Titin (Wang, 1996), the giant muscle protein, has not been known to contribute to the myosin filament intensities. The main components of the thin filament are the actin subunits, troponin, tropomyosin, and nebulin. The stochiometry of actin to troponin is 7:1. Troponin has a repeat of 38.5 nm, which is different from the actin repeat of 36.5 nm in the skeletal muscle. Tropomyosin is a continuous coiled-coil thread structure so that it diffracts as a continuous helix with Bessel function orders 2, 4, 6, 8, 10, 12, etc., on layer lines 1, 2, 3, 4, 5, 6, etc. In the small-angle x-ray diffraction patterns, it may be observed only in the outer region of ALL1 because the helical radius of the tropomyosin thread is between 37 and 41 Å (the first peak center of the intensity profile is ~0.013~0.014 $Å^{-1}$). Also, the mass of the tropomyosin is < 0.25 ((2×2×33kD)/(13×42kD)) of the actin in every 36.5 nm, so that the intensity of the tropomyosin is much less than 1/16 intensity of the actin, making little contribution on the first actin layer line. Nebulin would also diffract as a continuous helix at perhaps even higher angles than tropomyosin. Therefore, it is reasonable to disregard contributions originating from the associated proteins in our modeling.

There is some sampling on the first actomyosin layer line (Fig. 1 in Xu et al., accompanying paper). Besides being the only sampling visible in the diffraction pattern, the sampling is very weak. Therefore, we fitted the envelope of the profile rather than introducing more parameters, such as the number of the unit cells in the coherent domain. The meridional reflection at 215 Å was not fitted, as it arises from perturbations in the distribution of myosin heads (Malinchik and Lednev, 1992). It will be shown that the modeling results are not affected whether the perturbation was included or not.

There is no apparent sampling from either simple or superlattices on the experimental MLL1. For instance, in the data shown in Fig. 1 *A* of Xu et al. (accompanying paper), d_{10} spacing of the lattice is 404.5 Å. If there is sampling from a superlattice (Huxley and Brown, 1967; Squire, 1975), the profile of MLL1 should have peaks indexed [*hk*] on the superlattice at *10*, *20*, *21*, *31*, *40*, *32*, *50*, etc., which will correspond to the reciprocal spacings of 0.0014, 0.0029, 0.0038, 0.0052, 0.0057, 0.0062, and 0.0071 $Å^{-1}$. If there is sampling from the simple lattice, the profile of MLL1 will have peaks indexed [*hk*] at the reciprocal spacings of 0.0025, 0.0043, 0.0049, 0.0065, and 0.0089 $Å^{-1}$. However, the peaks of the experimental MLL1 are at 0.0033 and 0.0069 $Å^{-1}$. Neither of the two peaks can match either a simple or a superlattice. Moreover, if there is an effect of sampling, small peaks should appear in the first layer line profile indexed at higher orders of the superlattice, which were not observed in the experimental MLL1. Therefore, the effects of a superlattice, even if it does exist in the rabbit psoas muscle, are not significant.

(e) Calculations of the diffraction patterns

The diffraction pattern of the model is composed of two parts, one being the myosin filament, and the other being from the actin filament. The ratio of myosin filaments to actin filaments in the transverse section of the A-band is 1:2. Because there is an ensemble of filaments in the muscle cells, the layer lines of the observed fiber diffraction pattern from an unsampled collection of helical objects are the same as the cylindrically averaged layer lines of each individual filament. Myosin and actin helices are of different helical repeats. As there is no interference between Bessel

functions of different orders and if one does not consider interference from lattice sampling, the diffracted intensity of layer lines is represented by

$$I_l(R) = I_{M,l}(R) + I_{A1,l}(R) + I_{A2,l}(R)$$

where $I_{M,l}(R)$ is the intensity from the myosin filament. The backbone of the myosin filament is assumed not to contribute to the diffraction pattern except to the equatorial reflections. $I_{A1,l}(R)$ and $I_{A2,l}(R)$ are the intensities from the two actin filaments, contributed separately by individual actin filaments and their bound myosin heads. The intensity of each layer line (l) of the helix at the reciprocal radius (R) is the sum of the intensities of the individual Bessel orders on each layer line (Franklin and Klug, 1955),

$$\langle I_l(R)\rangle_\psi = \sum_n |F_{nl}(R)|^2$$

The Bessel orders (n) on the layer lines for the myosin helix are: on the first and fourth layer lines: 3, −6, 12; on the second and fifth: −3, 6, −12; on the third and sixth: 0, 9, −9. For actin helix they are: on the first: 2, −11, 15; on the second: 4, −9, 17; on the third: 6, −7, 19; on the fourth: −5, 8, −18; on the fifth: −3, 10, −16; and on the sixth: −1, 12, −14.

$$F_{nl}(R) = \sum_j f_j J_n(2\pi r_j R)\exp\left\{ i\left[n\left(\frac{\pi}{2} - \phi_j\right) + \frac{2\pi l z_j}{c}\right]\right\}$$

Where r_j, ϕ_j, and z_j are cylindrical coordinates of the jth sphere; f_j is the structural factor of the sphere with radii a_j.

$$f_j = 4\pi a_j^3 \frac{\sin(2\pi a_j\rho) - (2\pi a_j\rho)\cos(2\pi a_j\rho)}{(2\pi a_j\rho)^3}$$

where ρ is the distance from the origin in the reciprocal space.

(f) Selection of a binding pair

Because the reach of a myosin head is constrained by the lattice geometry, it is reasonable to assume that the head can only bind to the nearby actin subunits. To simulate attachment of a myosin head to actin, three models of attachment were considered. For each of the models, we first select a binding pair, defined as a myosin lattice point to a selected actin subunit in a neighboring actin filament. Starting from a myosin lattice point with radius R from the axis of the myosin filament, a search consisted of an area ±216 Å in the axial direction and ±60° in the azimuthal direction. For models A and B the nearest actin subunit from the myosin lattice point was chosen to form the binding pairs. For model C, instead of the nearest neighbors, the actin subunit was selected at a distance closest to the chord length of the myosin head (from the tail end to the binding site on the motor domain, ~137 Å). Because of the mismatch of the periodicities of the filaments, the distances between the binding pairs differ from one another. For myosin to attach to actin, it must fit into the space defined for the binding pair. Because some flexibility within the myosin head or within some other parts of the myosin filament assembly is required, subsequent variations were made for the three models.

Model A. After an actin subunit is selected, the myosin head is connected to the actin forming a binding pair at an angle α to the z axis and an azimuthal angle β with respect to the actin filament (Fig. 1). To fit into the space between the filament surfaces, the radial position R of the S1-S2 junction at the helical lattice point is allowed to deviate ΔR whereas the shape of myosin head remains unchanged.

Model B also finds the shortest distance between the myosin lattice point and the actin subunit. However, to fit the shortest distance, the myosin head changes its conformation approximately at the converter region (Houdusse et al., 1999), such that the angle (ψ) between the light chain binding domain and the binding site in the motor domain is a variable (Fig. 1), but the position of the tail end is kept at the helical lattice point.

Model C lets the chord length of the myosin head (~137 Å) select the corresponding actin for the binding pair. Subsequently, as in model A, binding was accomplished by adjusting the radial position of the S1-S2 junction at the myosin lattice point, while keeping the shape of S1 unchanged.

(g) Location of the second head

Some extra mass associated with the attached myosin head was found necessary to improve the fitting of the experimental data. As a reasonable assumption, the extra mass was modeled as the second head of the cross-bridge. The second head (H2) is connected with the first at the end of the tail domain. The structure and the mass of the second head are assumed to be identical to the first one. The disposition of the second head is affected by the position of the first head so that it is in some degree of an ordered state when the first head is attached to an actin. The orientation of the second head is defined by a uniform azimuthal angle φ in the XOY plane perpendicular to the z axis and γ angle projected onto the XOY plane (Fig. 1). The H2 also follows the first head in Z-direction, which points toward either the Z-line or the M-line, but the γ angle is independent to the first head. For simplicity, the H2 did not rotate around its own axis.

(h) Model parameters

The following parameters and constraints were used in search for the best fit for the experimental data:

A binding pair = a myosin at helical lattice point paired with a selected actin subunit in an actin filament. To select a binding pair, from each lattice point on the myosin filament, a search routine was performed in the range of ±216 Å in the axial direction and ±60° in the azimuthal direction; separate selection criteria were set for models A, B, or C.

R = the radius of the helical lattice point on the myosin filament. It was varied between 75 and 135 Å in the iterative process of finding a binding pair that results in an interim best fit to experimental data.

ΔR = adjustment in R used in models A and C; after the binding pair was selected, the position of the tail end of S1 (the center of the last sphere of S1, ~S1-S2 junction) was assumed to be at R; for S1 to fit into the space as determined for a binding pair, the radial position was further adjusted by ΔR. If ($R + \Delta R$) is less than the radius of the backbone (75 Å), the selection was rejected.

ψ = the angle between the light chain domain and the binding site in the motor domain of S1; ψ was fixed at 134.9 in models A and C, but no limit was placed on its range in model B.

r = the radial position of the binding site on the actin subunit from the axis of the actin filament; it was varied between 25 and 55 Å.

θ = the azimuthal angle of binding site on actin with the putative rigor binding site being set as $\Delta\theta = 0°$; $\Delta\theta$ was varied between −15 and 45°.

z = the axial position of binding site on actin with the putative rigor binding site being set as the origin; it was varied between 0 and 55 Å.

γ = the angular disposition in the axial direction of the second myosin head with respect to the plane perpendicular to the z axis; it was varied between 0 and ± 30°.

φ = the azimuthal angular disposition of the second myosin head projected onto the plane perpendicular to the z-axis; it was varied between 60 and 140°.

Constraints on the search for a binding pair = ± 216 Å in the axial (Z) direction; ± 60° in the azimuthal direction.

(i) Calculation procedures

1. Find the binding pairs. Starting at a given myosin lattice point, at an initial radius R from the center of the myosin filament, a search was performed for an appropriate actin subunit with binding site at radius r with

respect to the axis of the actin filament. z and θ were also kept constant during this step, restricting the binding site on each actin subunit to just one of several sites which might be compatible with a chosen r value. The distance between a binding pair was required to satisfy the individual model assumptions: for model A, the shortest distance; for model B, also the shortest distance; and for model C, the distance closest to the chord length of S1 (~135 Å).

2. Place S1 between the two endpoints found in step 1, with the small sphere at the tip as the actin binding site and the last sphere as the tail end. To fit the S1 into the binding pair distance, adjustments were made according to the assumptions for the three models. For model A, the radial position R at the tail end was further adjusted by ΔR such that the conformation of S1 was not changed. For model B, the angle Ψ was varied, but R was kept constant. For model C, R of the tail end was further adjusted by ΔR such that the conformation of S1 was not changed.

3. Steps 1 and 2 were repeated by systematically varying R, ΔR, and r, until an intermediate best fit was selected by visually judging the overall fitting of MLL1 and ALL1, at the first peak position and the shape of the MLL1.

4. The second head was then added in the calculations with the last spheres of the two S1 joined; starting with the second head assuming the same orientation as the first head and then the two parameters γ and φ were varied. After steps 3 and 4, we checked the validity of the selected r and R by repeating steps 1 and 2.

5. The fit was further improved by rotating the actin filament through varying the angle θ and the axial distance z with $\Delta\theta$ and Δz. Steps 1 and 2 were repeated to further optimize the selected model A.

6. The resultant attachment orientations of the myosin heads are expressed in the tilt angle α and slew angle β relative to the axis of the actin. For model B, there is a distribution in ψ, the angle between the light chain domain and the binding site in the motor domain of S1.

The authors thank Dr. Gerald Offer for his critical reading of the manuscript.

REFERENCES

Barnett, V. A., and M. Schoenberg. 1993. The strength of binding of the weakly-binding crossbridge created by sulfhydryl modification has very low calcium sensitivity. *Adv. Exp. Med. Biol.* 332:133–140.

Brenner, B., L. C. Yu, and J. M. Chalovich. 1991. Parallel inhibition of active force and relaxed fiber stiffness in skeletal muscle by caldesmon: implications for the pathway to force generation. *Proc. Natl. Acad. Sci. U.S.A.* 88:5739–5743.

Chalovich, J. M., P. B. Chock, and E. Eisenberg. 1981. Mechanism of action of troponin-tropomyosin. *J. Biol. Chem.* 256:575–578.

Chalovich, J. M., and E. Eisenberg. 1982. Inhibition of actomyosin ATPase activity by troponin-tropomyosin without blocking the binding of myosin to actin. *J. Biol. Chem.* 257:2432–2437.

Chalovich, J. M., and E. Eisenberg. 1986. The effect of troponin tropomyosin on the binding of heavy meromyosin to actin in the presence of ATP. *J. Biol. Chem.* 261:5088–5093.

Dominguez, R., Y. Freyzon, K. M. Trybus, and C. Cohen. 1998. Crystal structure of a vertebrate smooth muscle myosin motor domain and its complex with the essential light chain: visualization of the pre-power stroke state. *Cell.* 94:559–571.

Eisenberg, E., and T. L. Hill. 1985. Muscle contraction and free energy transduction in biological systems. *Science.* 227:999–1006.

Fisher, A. J., C. A. Smith, J. B. Thoden, R. Smith, K. Sutoh, H. M. Holden, and I. Rayment. 1995. X-ray structures of the myosin motor domain of *Dictyostelium discoideum* complexed with MgADP·BeFx and MgADP·AlF4-. *Biochemistry.* 34:8960–8972.

Frado, L.-L., and R. Craig. 1992. Electron microscopy of the actin-myosin head complex in the presence of ATP. *J. Mol. Biol.* 223:391–397.

Franklin, R. E., and A. Klug. 1955. The splitting of layer-lines in X-ray fibre diagrams of helical structures. Applications to tobacco mosaic virus. *Acta Crystallogr.* 8:777–780.

Gu, J., S. Xu, and L. C. Yu. 2000. Modeling the weakly attached cross-bridges in the A.M.ATP state. *Biophys. J.* 78:231A.

Gu, J., and L. C. Yu. 1999. X-ray diffraction of helices with arbitrary periodic ligand binding. *Acta Crystallogr. D.* 55:2022–2027.

Hansen, J. E., J. Marner, D. Pavlov, P. A. Rubenstein, and E. Reisler. 2000. Structural transition at actin's N-terminus in the actomyosin cross-bridge cycle. *Biochemistry.* 39:1792–1799.

Hirose, K., and T. Wakabayashi. 1988. Thin filaments of rabbit skeletal muscle are in helical register. *J. Mol. Biol.* 204:797–801.

Houdusse, A., V. N. Kalabokis, D. Himmel, A. G. Szent-Gyorgyi, and C. Cohen. 1999. Atomic structure of scallop myosin subfragment S1 complexed with MgADP: a novel conformation of the myosin head. *Cell.* 97:459–470.

Houdusse, A., A. G. Szent-Gyorgyi, and C. Cohen. 2000. Three conformational states of scallop myosin S1. *Proc. Natl. Acad. Sci. U.S.A.* 97:11238–11243.

Huxley, H. E., and W. Brown. 1967. The low-angle x-ray diagram of vertebrate striated muscle and its behaviour during contraction and rigor. *J. Mol. Biol.* 30:383–434.

Kabsch, W., H. G. Mannherz, D. Suck, E. F. Pai, and K. C. Holmes. 1990. Atomic structure of the actin: DNase I complex. *Nature.* 347:37–44.

Kim, D. S., Y. Takezawa, M. Ogino, T. Kobayashi, T. Arata, and K. Wakabayashi. 1998. X-ray diffraction studies on the structural changes of rigor muscles induced by binding of phosphate analogs in the presence of MgADP. *Biophys. Chem.* 74:71–82.

Juanhuix, J., J. Bordas, J. Campmany, A. Svensson, M. L. Bassford, and T. Narayanan. 2001. Axial disposition of myosin heads in isometrically contracting muscles. *Biophys. J.* 80:1429–1441.

Kraft, T., J. M. Chalovich, L. C. Yu, and B. Brenner. 1995. Parallel inhibition of active force and relaxed fiber stiffness by Caldesmon fragments at physiological ionic strength and temperature conditions: additional evidence that weak cross-bridge binding to actin is an essential intermediate for force generation. *Biophys. J.* 68:2404–2418.

Lehman, W., R. Craig, and P. Vibert. 1994. Ca^{2+}-induced tropomyosin movement in Limulus thin filaments revealed by three-dimensional reconstruction. *Nature.* 368:6466–6467.

Linari, M., L. Lucii, M. Reconditi, M. E. Casoni, H. Amenitsch, S. Bernstorff, G. Piazzesi, and V. Lombardi. 2000. A combined mechanical and X-ray diffraction study of stretch potentiation in single frog muscle fibres. *J. Physiol.* 526:589–596.

Lowy, J., D. Popp, and A. A. Stewart. 1991. X-ray studies of order-disorder transitions in the myosin heads of skinned rabbit psoas muscles. *Biophys. J.* 60:812–824.

Malinchik, S. B., and V. V. Lednev. 1992. Interpretation of the X-ray diffraction pattern from relaxed skeletal muscle and modelling of the thick filament structure. *J. Muscle Res. Cell Motil.* 13:406–419.

Malinchik, S., S. Xu, and L. C. Yu. 1997. Temperature-induced structural changes in the myosin thick filament of skinned rabbit psoas muscle. *Biophys. J.* 73:2304–2312.

Mendelson, R., and E. P. Morris. 1997. The structure of the acto-myosin subfragment 1 complex: results of searches using data from electron microscopy and x-ray crystallography. *Proc. Natl. Acad. Sci. U.S.A.* 94:8533–8538.

Rayment, I., W. Rypniewski, K. Schmidt-Base, R. Smith, D. R. Tomchick, M. M. Benning, D. A. Winkelmann, G. Wesenberg, and H. M. Holden. 1993a. Three-dimensional structure of myosin subfragment-1: a molecular motor. *Science.* 261:50–58.

Rayment, I., H. M. Holden, M. Whittaker, C. B. Yohn, M. Lorenz, K. C. Holmes, and R. A. Milligan. 1993b. Structure of the actin-myosin complex and its implications for muscle contraction. *Science.* 261: 58–65.

Rayment, I., C. Smith, and R. G. Yount. 1996. The active site of myosin. *Annu. Rev. Physiol.* 58:671–702.

Rome, E., G. Offer, and F. A. Pepe. 1973. X-ray diffraction of muscle labelled with antibody to C-protein. *Nat. New Biol.* 244:152–154.

Schroder, R. R., D. J. Manstein, W. Jahn, H. Holden, I. Rayment, K. C. Holmes, and J. A. Spudich. 1993. Three-dimensional atomic model of F-actin decorated with *Dictyostelium* myosin S1. *Nature.* 364:171–174.

Smith, C. A., and I. Rayment. 1996. X-ray structure of the magnesium(II). ADP.vanadate complex of the *Dictyostelium discoideum* myosin motor domain to 1.9 A resolution. *Biochemistry.* 35:5404–5417.

Squire, J. M. 1975. Muscle filament structure and muscle contraction. *Annu. Rev. Biophys. Bioeng.* 4:137–163.

Squire, J. M., J. J. Harford, A. C. Edman, and M. Sjostrom. 1982. Fine structure of the A-band in cryo-sections. III. Crossbridge distribution and the axial structure of the human C-zone. *J. Mol. Biol.* 155:467–494.

Squire, J. M., H. A. al-Khayat, and N. Yagi. 1993. Muscle thin-filament structure and regulation, actin sub-domain movements and the tropomyosin shift modeled from low-angle X-ray diffraction. *J. Chem. Soc. Faraday Trans.* 89:2717–2726.

Stewart, M., and R. W. Kensler. 1986. Arrangement of myosin heads in relaxed thick filaments from frog skeletal muscle. *J. Mol. Biol.* 192: 831–851.

Sutoh, K. 1982. Identification of myosin-binding sites on the actin sequence. *Biochemistry.* 21:3654–3661.

Taylor, K. A., H. Schmitz, M. C. Reedy, Y. E. Goldman, C. Franzini-Armstrong, H. Sasaki, R. T. Tregear, K. Poole, C. Lucaveche, R. J. Edwards, L. F. Chen, H. Winkler, and M. K. Reedy. 1999. Tomographic 3D reconstruction of quick-frozen, Ca^{2+}-activated contracting insect flight muscle. *Cell.* 99:421–431.

Wang, K. 1996. Titin/connectin and nebulin: giant protein rulers of muscle structure and function. *Adv. Biophys.* 33:123–134.

White, H., B. Belknap, and M. R. Webb. 1997. Kinetics of nucleoside triphosphate cleavage and phosphate release steps by associated rabbit skeletal actomyosin, measured using a novel fluorescent probe for phosphate. *Biochemistry.* 36:11828–11836.

Xie, L., W. X. Li, T. Rhodes, H. White, and M. Schoenberg. 1999. Transient kinetic analysis of N-phenylmaleimide-reacted myosin subfragment-1. *Biochemistry.* 38:5925–5931.

Xu, S., J. Gu, G. Melvin, and L. C. Yu. 2001. Evidence that the conformation of the actomyosin complex with bound ADP·Pi (the A·M·ADP·Pi state) differs from that in the A·M·ATP state. *Biophys. J.* 80:267a.

Xu, S., S. Malinchik, T. Kraft, B. Brenner, and L. C. Yu. 1997. X-ray diffraction studies of cross-bridges weakly bound to actin in relaxed skinned fibers of rabbit psoas muscle. *Biophys. J.* 73:2655–2666.

Xu, S., L. C. Yu, and M. Schoenberg. 1998. Behavior of N-phenylmaleimide-reacted muscle fibers in magnesium-free rigor solution. *Biophys. J.* 74:1110–1114.

Xu, S., J. Gu, G. Melvin, and L. C. Yu. 2002. Structural characterization of weakly attached cross-bridges in the A·M·ATP state in permeabilized rabbit psoas muscle. *Biophys. J* 82:2111–2122.

Xu, S., J. Gu, T. Rhodes, B. Belknap, G. Rosenbaum, G. Offer, H. White, and L. C. Yu. 1999. The M·ADP·P(i) state is required for helical order in the thick filaments of skeletal muscle. *Biophys. J.* 77:2665–2676.